M-shell x-ray production by 0.6–4.0-MeV protons in ten elements from hafnium to thorium

M. Pajek
Institute of Physics, Pedagogical University, 25-509 Kielce, Poland

A. P. Kobzev, R. Sandrik, and A. V. Skrypnik
Joint Institute for Nuclear Research, Dubna, U.S.S.R.

R. A. Ilkhamov and S. H. Khusmurodov
Institute of Applied Physics, Tashkent State University, Tashkent, U.S.S.R.

G. Lapicki
Department of Physics, East Carolina University, Greenville, North Carolina 27858
(Received 1 December 1989)

M-shell x-ray production cross sections for selected heavy elements, namely, $_{72}$Hf, $_{73}$Ta, $_{74}$W, $_{75}$Re, $_{76}$Os, $_{77}$Ir, $_{78}$Pt, $_{79}$Au, $_{83}$Bi, and $_{90}$Th, were measured for protons of energy 0.6–4.0 MeV. The experimental results are compared with the predictions of the first Born and semiclassical approximations for M-shell ionization; these data are also compared with the theory that accounts for the projectile's energy loss and Coulomb deflection as well as for the target's M-shell electron perturbed stationary state and relativistic nature (ECPSSR). Generally, fair agreement between the data and the ECPSSR theory is found. Some systematical discrepancies observed for the lightest elements (Hf, Ta, and W) are explained as possible ambiguities in the M-shell Coster-Kronig factors and fluorescence yields, which were used to convert theoretical M-subshell ionization cross sections to the total M-x-ray production cross sections. The experimental total M-shell ionization cross sections were obtained from measured M-x-ray cross sections using the proposed approximate average fluorescence yield $\bar{\omega}_M$ that relies on two fluorescence yields and the Coster-Kronig factor for *only* M_4 and M_5 subshells.

I. INTRODUCTION

Atomic inner-shell ionization by charged particle impact has been studied extensively in recent decades due to importance of this phenomenon for both applications [e.g., the particle induced x-ray emission (PIXE) method] and in theory (i.e., for developing more reliable theoretical models describing this fundamental process of interaction of ions with matter). The direct Coulomb ionization, being the dominant mechanism of the inner-shell vacancy production in asymmetric collisions ($Z_1 \ll Z_2$, where Z_1 and Z_2 are projectile and target atomic numbers, respectively), may be described in the first-order plane-wave Born[1] (PWBA) and the semiclassical[2] (SCA) approximations. The ECPSSR theory of Brandt and Lapicki[3] includes higher-order corrections for the energy loss, Coulomb deflection, binding-polarization, and relativistic effects, and hence it goes beyond the first-order schemes.[1,2]

Most of the experimental studies concerning inner-shell ionization by ion impact were limited to the K shell[4] and the L shell,[5] while relatively few measurements were performed for the M shell. In early M-shell ionization experiments the flow-proportional counters were used;[6–9] more precise measurements of cross sections became available with the use of high-resolution Si(Li) detectors.[10–25] However, most of these M-shell studies were performed for MeV-ion impact on a few elements only—most often gold (Refs. 6, 8, 10, 11, 13, 14, 17–21, 24, and 25) and bismuth (Refs. 6, 8, 13–15, 18, 20, 21, 24, and 25)—and, additionally, large discrepancies (up to a factor of 2) between the data reported by different authors exist. This situation is probably connected with two essential difficulties arising in measurements of M-shell x-ray production cross sections by ion bombardment. First, the Si(Li) detector efficiency should be accurately known for the low-energy x rays (below 4 keV), which is difficult to estimate, and second, thin, contamination-free carbon target backings must be used to avoid any interference between M x rays of studied elements with K x rays of light target atoms occurring as contaminants in the carbon backings.

In this paper, we report on systematical measurements of M-shell x-ray production cross sections for selected heavy elements ($72 \leq Z_2 \leq 90$) by 0.6–4.0 MeV protons. A precision low-energy Si(Li) detector efficiency determination[26] was used in the present study and the target carbon backing purity was controlled by the PIXE method, which allows us to reduce total experimental uncertainties to a level of 7–10 %.

Experimental methods to obtain and analyze the data are in Sec. II, while Sec. III lists M-shell ionization theories and addresses the question of a proper choice of M-shell fluorescence and Coster-Kronig yields. Our data

are shown and compared in Sec. IV with experimental cross sections of other workers and with theoretical *M*-subshell ionization cross sections converted to *M*-x-ray production cross sections. Conclusions are made in Sec. V.

II. MEASUREMENTS AND DATA ANALYSIS

Proton beams of 0.6–4.0 MeV from the EG-5 Van de Graaff accelerator at JINR, Dubna, have been used in the present experiment. The collimated beam of 1.5 mm diameter was directed onto thin targets tilted at an angle 45° relative to the beam direction. An x-ray Si(Li) detector, having the resolution of 220 eV at 6.4 keV, was placed perpendicular to the beam axis, outside the experimental chamber with a 25-μm-thick, Al-metallized, Mylar window. Consequently, the x-ray absorption both in the window and in the 10-mm air gap between the chamber and Si(Li) detector windows were carefully calibrated and included in the total efficiency of the Si(Li) detector (for details see discussion below and Ref. 26). A silicon surface barrier detector was positioned at an angle of 135° relative to the beam direction. The target and the graphite cylinder surrounding target holder were connected with the Faraday cup for beam current integration. An additional graphite cylinder, kept at potential -300 V, was used to suppress the secondary electron escape from the target. The standard data acquisition system with pile-up and dead-time corrections, interfaced to microcomputer for data storage, was employed for both x-ray and charged-particle signals.

The special care was devoted to accurate efficiency determination of the Si(Li) detector because of the Si-*K* and Au-*M* absorption edge structure in the efficiency curve in the x-ray energy region corresponding to *M* x rays of heavy elements studied in the present work, i.e., 1.5–4 keV. The Si(Li) detector efficiency was measured in two ways: for soft x rays by a PIXE method using ^{1}H- and ^{4}He-ion impact and for higher x-ray energies using ^{57}Co and ^{241}Am sources. The experimental efficiency was further analyzed according to the procedure described in detail by Pajek *et al.*[26] that calls for an accurate determination of the thicknesses of Au detector contact, Si dead layer, and contamination (mainly ice) layer on the front surface of Si crystal. Also, according to the proposed Si(Li) detector model,[26] the increased peripheral Si dead layer (called the "edge effect") was taken into account. The measured intrinsic efficiency of the Si(Li) detector used in the present study is shown in Fig. 1, where the estimated detector parameters are displayed. The application of the Si(Li) detector calibration procedure mentioned above allowed us to determine the Si(Li) detector efficiency with 7–3 % uncertainties in the x-ray energy region of 1.5–4 keV, respectively.

Typical spectra of x-rays and elastically scattered projectiles for 2-MeV protons on the Au target are shown in

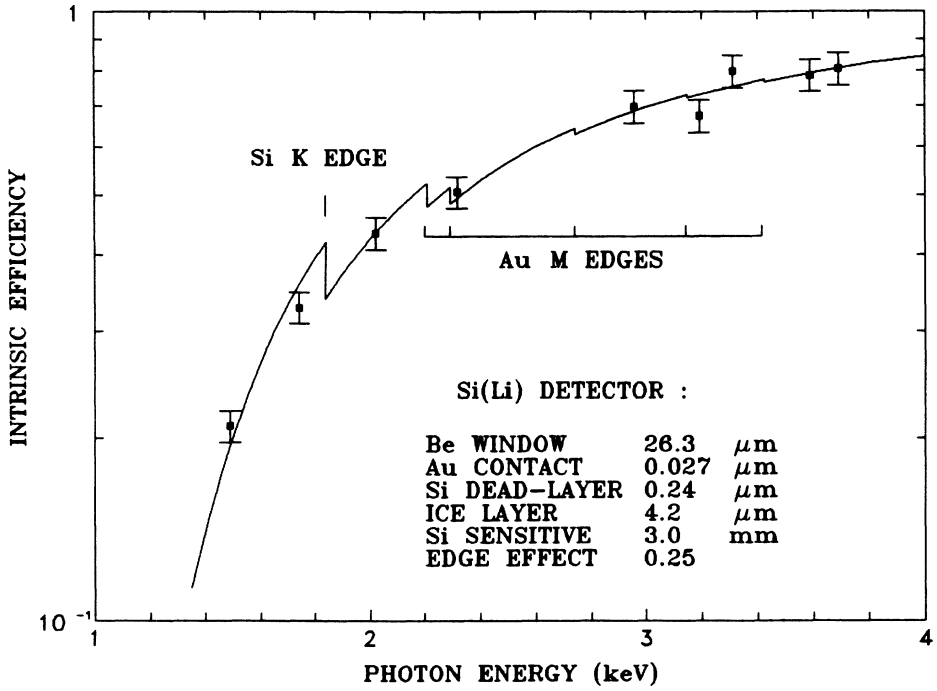

FIG. 1. Experimental (■) and fitted (——) low-energy intrinsic efficiency of the Si(Li) detector used in the present work, plotted vs photon energy. A detailed description of the fitted curve and detector parameters is discussed in Ref. 26. The estimated values of detector parameters are displayed in the figure.

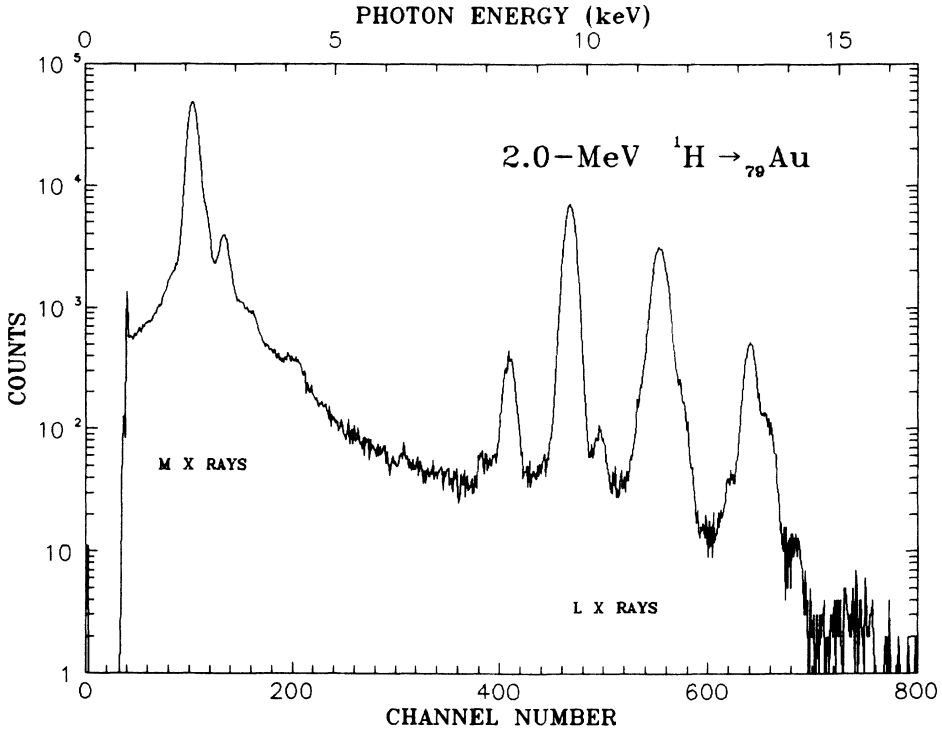

FIG. 2. X-ray spectrum of the $_{79}$Au target for 2-MeV protons.

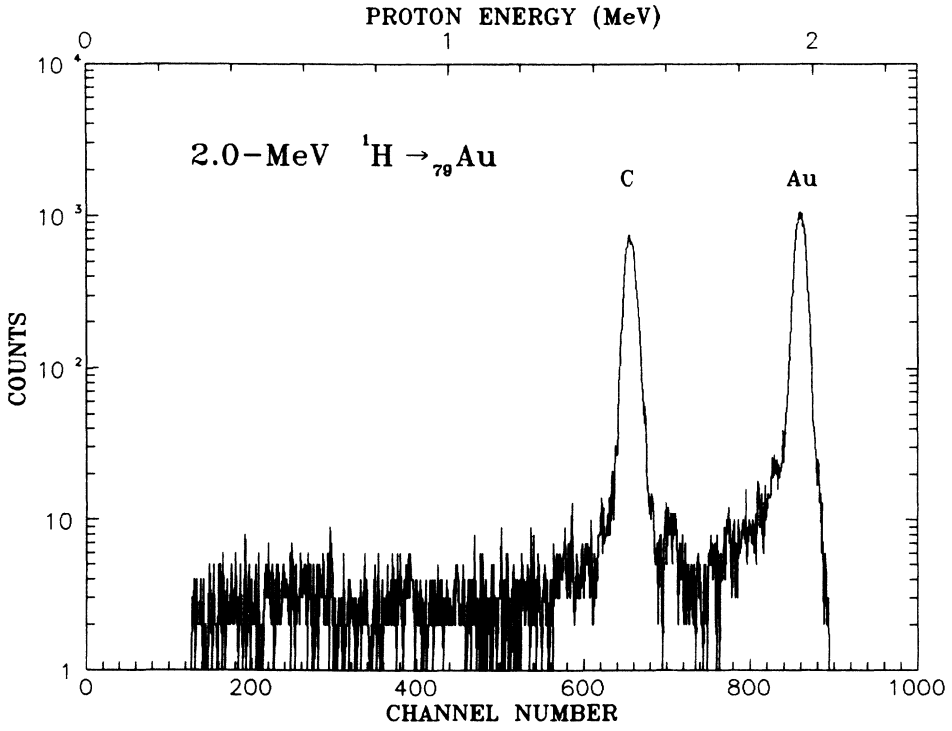

FIG. 3. Spectrum of the protons elastically scattered on the $_{79}$Au target for 2-MeV protons.

Figs. 2 and 3, respectively. As can be seen from Fig. 2 the Au M-x-ray spectrum, being typical for studied elements, cannot be resolved into all individual x-ray transitions using a Si(Li) detector, but only complex dominating x-ray lines may be separated experimentally. The measured x-ray spectra were analyzed, assuming a Gaussian line shape for the full energy x-ray peaks and a polynomial background, by a nonlinear least-square fitting method using the program ACTIV.[27] However, to determine precisely the areas of the dominating M-x-ray lines we have used this program in an iterative mode consisting of subsequent energy calibration, peak fitting and energy calibration refinement for the increasing number of x-ray lines to be analyzed. After three steps of this procedure seven dominating M-x-ray lines of interest [i.e., $M_\zeta(M_{4,5}N_{2,3})$, $M_3N_1+M_4N_3$, $M_{\alpha\beta}(M_{4,5}N_{6,7})$, $M_\gamma(M_3N_5)$, $M_3O_{4,5}+M_2N_2$, M_2O_4, and $M_1O_{2,3}$] emerged and were fitted as shown (in a Au M-x-ray spectrum for 2-MeV protons) in Fig. 4, where dominating M-x-ray lines are identified.

The experimental x-ray production cross section $\sigma_x(E_1)$ for an individual x-ray line of the energy E_x and for the projectile energy E_1 is given by

$$\sigma_x(E_1)=\frac{N_x}{\varepsilon_{\text{tot}}(E_x)N_p}\sigma_{\text{el}}(E_1)\Omega_d F(E_1,\Delta E)\ , \tag{1}$$

where N_x and N_p are the numbers (dead-time corrected) of the x rays and elastically scattered protons, respectively; $\varepsilon_{\text{tot}}(E_x)$ is the total efficiency of the Si(Li) detector for x-ray energy E_x; and $\sigma_{\text{el}}(E_1)$ is the differential elastic cross section into Ω_d, which denotes the surface-barrier detector solid angle. The factor $F(E_1,\Delta E)$ accounts for a finite target thickness that results both in x-ray absorption and projectile energy loss ΔE in the target. The magnitude of this correction—assuming that the x-ray production cross section and stopping power $S(E_1)$ depend on energy as E_1^α and E_1^β, respectively—may be estimated using simple correction factor (see also Ref. 26),

$$F(E_1,\Delta E)=\frac{1+\frac{1}{2}(\beta+2)\dfrac{\Delta E}{E_1}}{1-\dfrac{1}{2}\left[\alpha-\beta+\dfrac{\mu E_1}{S(E_1)}\right]\dfrac{\Delta E}{E_1}}\ , \tag{2}$$

where the energy-loss ΔE is related to the target thickness Δx by a relation $\Delta E=\Delta x S(E_1)$ and the geometry of the present experiment is assumed, i.e., a 45° target tilt angle and Si(Li) detector perpendicular to the beam axis. For determination of β, the stopping power tables of Andersen and Ziegler[28] were adopted and the mass attenuation coefficients μ were extracted from Veigele.[29] The values of α were determined from measured cross sec-

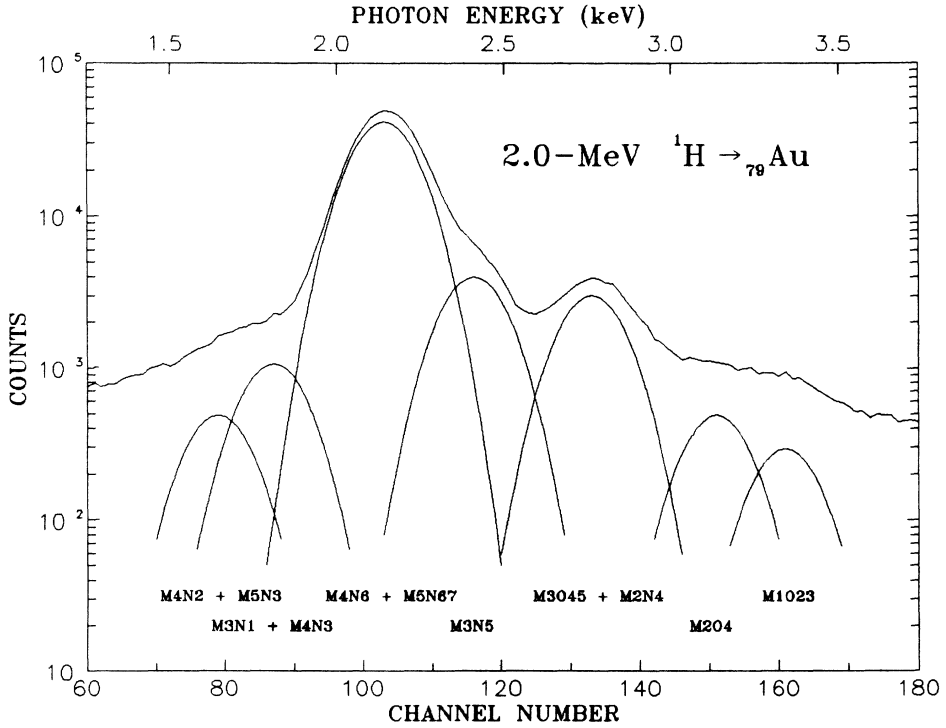

FIG. 4. M-shell x-ray spectrum of $_{79}$Au for 2-MeV protons as analyzed by the ACTIV program (Ref. 27). The resolved M-x-ray lines are indicated in the figure.

TABLE I. The measured M-shell x-ray production cross sections (in b), the total experimental uncertainties, target thicknesses Δx, and the average M-shell fluorescence yields $\bar{\omega}_M$ of Eq. (6) with Ref. 46.

Proton energy (MeV)	$_{72}$Hf	$_{73}$Ta	$_{74}$W	$_{75}$Re	$_{76}$Os
0.6	495	434	439	486	452
0.7	598	533	539	583	563
0.8	723	631	616	677	616
0.9	847	734	718	758	714
1.0	964	827	795	868	823
1.2	1280	1070	1040	1170	1050
1.4	1520	1310	1260	1340	1290
1.6	1800	1380	1360	1500	1430
1.8	1910	1600	1560	1710	1620
2.0	1980	1650	1700	1740	1720
2.2	2280	1990	1930	2020	1950
2.4	2400	2150	2050	2130	2110
2.6	2440	2160	2090	2200	2110
2.8	2460	2100	2230	2380	2280
3.0	2560	2240	2290	2370	2310
3.2	2630	2240	2370	2560	2380
3.4	2650	2390	2410	2570	2550
3.6				2670	2510
4.0					2700
Uncertainty (%)	8	8	8	10	10
Δx(μg/cm^2)	23	35	28	19	26
$\bar{\omega}_M$	0.0176	0.0187	0.0197	0.0210	0.0225

Proton energy (MeV)	$_{77}$Ir	$_{78}$Pt	$_{79}$Au	$_{83}$Bi	$_{90}$Th
0.6	410	394	382	282	152
0.7	512	490	485	351	198
0.8	601	553	542	400	244
0.9	702	647	629	472	284
1.0	755	700	673	546	347
1.2	973	889	876	636	394
1.4	1180	1040	1040	776	530
1.6	1280	1200	1240	944	627
1.8	1520	1420	1400	1090	733
2.0	1710	1630	1610	1260	851
2.2	1880	1800	1710	1330	968
2.4	2040	1930	1940	1610	1100
2.6	2230	2120	2070	1640	1200
2.8	2350	2220	2200	1830	1330
3.0	2410	2280	2300	1930	1370
3.2	2570	2430	2440	1840	1460
3.4	2660	2560	2500	1960	1570
3.6	2820	2620	2640	2000	1610
3.8	2780	2670	2640	2160	1650
4.0	2810	2640	2630	2090	1750
Uncertainty (%)	9	9	8	7	7
Δx(μg/cm^2)	23	23	27	31	2.7
$\bar{\omega}_M$	0.0238	0.0251	0.0266	0.0325	0.0448

tions using an iterative procedure to the α parameter derived from, first, uncorrected and then corrected in a preceding step, σ_x values, until the relative changes in α were negligible (less than 1%). Practically, two or three steps were sufficient in this iteration.

The elastic cross section $\sigma_{el}(E_1)$ in Eq. (1) is routinely assumed to be Rutherford. When the low-energy projectiles are scattered on heavy atoms, however, the screening effect[30,31] starts to be important. The screened elastic cross section according to Huttel *et al.*[31] was adopted in the present work.

The total M-x-ray cross sections σ_{MX} were obtained by adding σ_x of Eq. (1) for resolved M-x-ray lines mentioned above. It should be mentioned here, despite the fact that only total M-x-ray cross sections were finally derived, an accurate and precise estimation of the locations and intensities of dominating M-x-ray lines was of great importance due to a strong efficiency dependence on the M-x-ray energies for studied elements. Moreover, we have found that the intensity of a weak M_ζ line (about 4% of total M-x-ray intensity) was probably affected by a tail artifact[32] connected with strong $M_{\alpha\beta}$ line. The M_ζ-x-ray cross sections were thus estimated from experimental $M_{\alpha\beta}$ ones (originated from the same $M_{4,5}$ subshells decay), given that the ratio $M_\zeta/M_{\alpha\beta}$ may be evaluated using M-shell emission rates of Chen *et al.*[33]

The targets used in the experiment consisted of a thin (2.7–35 μg/cm^2; see Table I) layer of studied element evaporated onto thin (20 μg/cm^2) carbon foil using electron-gun evaporation technique. The preparation of the contamination-free carbon foils was a crucial point of the present experiment, to avoid any interference between M-x-rays of interest and K x-rays of typical, light contaminations present in carbon foils.[34] We have minimized this problem, controlling the preliminary contamination level in carbon foils by PIXE method using 3-MeV protons.

Another possible problem arising in estimation of the total M-shell x-ray production cross sections is a nonisotropic emission of x rays following M_3, M_4, and M_5 vacancy decay, due to an alignment effect.[35] The M-shell alignment in thorium for proton impact of energy 0.15–4 MeV has been studied by Wigger *et al.*[36] Using their values of the alignment parameter $\mathcal{A}_{20}(E_1)$, which are practically independent on the target atomic number,[37] we estimate, that for studied elements the influence of M-shell alignment on the measured total M-x-ray cross sections is less than 1% in the 0.6–4 MeV energy range of interest.

The total uncertainties of the measured M-shell x-ray cross sections are 7–10% (see Table I). They were caused, mainly, by the 3–7% uncertainty of the Si(Li) detector efficiency determination (see also Ref. 26). The statistical uncertainties for x-ray and elastic scattering yields (typically 1–2%) have practically no influence on final uncertainties of measured cross sections. The uncertainties of the particle detector solid angle and of the elastic cross sections (through an uncertainty of the particle detector angle ϑ) were canceled out because the Si(Li) detector efficiency $\varepsilon_{tot}(E_x)$ has been determined by the PIXE method in the same geometry.[26] The possible systematical errors, assumed to be 3% (due to, for example, not fully resolved M-x-ray transition structure) were taken also into account and combined linearly with statistical errors. The total uncertainties of the M-shell x-ray production cross sections were found to be nearly constant over the proton energy range of interest and their average values for studied elements are listed in Table I.

III. THEORIES FOR M-SHELL IONIZATION AND AVERAGE FLUORESCENCE YIELD

The direct Coulomb ionization, i.e., the excitation of inner-shell electron from a bound state to the continuum, is the dominating mechanism of the inner-shell vacancy production for strongly asymmetric ($Z_1 \ll Z_2$) systems. This process can be described using the first-order plane-wave Born approximation (PWBA).[1] According to the standard execution[38] of this approach, the M_i-subshell ionization cross sections may be expressed in terms of two dimensionless parameters, namely, the reduced binding energy $\theta_{M_i}=n^2E_{M_i}/Z_{2M_i}^2\mathcal{R}$ and the scaled velocity $\xi_{M_i}=2v_1/v_{2M_i}\theta_{M_i}$, where E_{M_i} is the experimental binding energy, $n=3$ is the principal quantum number, Z_{2M_i} is the effective target atomic number determined using Slater's screening constants: $Z_{2M_i}=Z_2-s_{M_i}$, with $s_{M_i}=11.25$ or 21.15 for M_1, M_2, and M_3 or M_4 and M_5 subshells, respectively; and $\mathcal{R}$ is the Rydberg constant. The v_1 and v_{2M_i} are the projectile and the screened hydrogenic inner-shell electron velocities. Using these parameters, the M_i-subshell ionization cross section in the PWBA approximation may be expressed as follows [see Eq. (1) of Ref. 38]:

$$\sigma_{M_i}^{PWBA}=\sigma_{0M_i}F_{M_i}(\xi_{M_i}^2/4n^2,\theta_{M_i})/\theta_{M_i}\ , \tag{3}$$

where $\sigma_{0M_i}\equiv 8\pi a_0^2Z_1^2Z_{2M_i}^{-4}$ and the $F_{M_i}(\xi_{M_i}^2/4n^2\theta_{M_i})$ function may be found in Ref. 38. Furthermore, the M-shell ionization process is dominated by the M_4- and M_5-subshell ionization and M_5 subshell ionization and the average reduced binding energy θ_M for heavy elements is nearly constant (e.g., $\theta_M=0.43$–0.47 for the $Z_2=72$–90 elements studied here), so that the normalized M-shell ionization cross sections σ_M/σ_{0M} may be described, practically, by a universal[38,39] function of average scaled velocity ξ_M, where σ_{0M} denotes an average value of σ_{0M_i} introduced in Eq. (3).

The electron capture to the projectile process also contributes to the M-shell vacancy production, especially for the systems with larger values of the ratio Z_1/Z_2 and lower energies.[40,41] Cross sections for this process may be described in the first Born approximation using the Oppenheimer-Brinkman-Kramers approach of Nikolaev[42] (OBKN).

Both direct ionization and electron-capture processes can be described in the ECPSSR theory as developed, correspondingly, by Brandt and Lapicki[3] and Lapicki and McDaniel.[40] On the other hand, only the direct M-shell ionization cross sections may be calculated using semiclassical approximation (SCA) with the straight-line tra-

jectory tables of Hansteen *et al.*[43] However, in these calculations, the corrections for higher-order effects have not been developed systematically for the M-shell and, as indicated in Ref. 38, the SCA tables[43] might have a numerical error. The M-shell x-ray production cross section σ_{MX} is related to the subshell ionization cross sections σ_{M_i} by the following relation:

$$\sigma_{MX} = \sum_{i=1}^{5} \nu_i \sigma_{M_i} , \tag{4}$$

where the effective M-shell fluorescence yields ν_i are defined[44] in terms of the fluorescence yields ω_i and Coster-Kronig factors f_{ij}. Moreover, the total M-shell x-ray production cross section may be related to the total M-shell ionization cross section σ_M by the relation $\sigma_{MX} = \bar{\omega}_M \sigma_M$, where $\bar{\omega}_M$ is the average M-shell fluorescence yield defined as

$$\bar{\omega}_M = \sum_{i=1}^{5} w_i \nu_i , \tag{5}$$

where $w_i \equiv \sigma_{M_i}/\sigma_M$ are the weights of the initial M-subshell vacancy distribution. In spite of rather strong variations of ω_i and f_{ij} with Z_2, the ν_i are within a few percent of each other for a given Z_2 in the $72 \leq Z_2 \leq 90$ range. Hence, as noted by Krause[45] in calculations of $\bar{\omega}_L$, the average inner-shell fluorescence yield such as $\bar{\omega}_M$ of Eq. (5) has a weak dependence on the chosen set $[w_1, w_2, w_3, w_4, w_5]$. According to both the first Born and ECPSSR calculations for all targets studied here, M_4 and M_5 subshells contribute to σ_M from some 80% to 70% in the 0.6–4 MeV range, respectively. Thus we find that

$$\bar{\omega}_M = 0.4(\omega_4 + f_{45}\omega_5) + 0.6\omega_5 , \tag{6}$$

corresponding to an extreme [0, 0, 0, 0.4, 0.6] initial vacancy distribution, where only dominating in ionization process M_4 and M_5 subshells, weighted by their degeneracy contribute, yields $\sigma_{MX} = \bar{\omega}_M \sigma_M$ to within 1% of what would have been obtained if the more involved Eq. (4) were to be used instead. We have used $\bar{\omega}_M$ of Eq. (6) (see Table I) to convert measured M-shell x-ray production cross sections to total M-shell ionization cross sections. As will be discussed in Sec. IV, the M-shell fluorescence yields and Coster-Kronig factors of Chen *et al.*[46] were used in the present work to calculate theoretical σ_{MX} cross sections of Eq. (4) and $\bar{\omega}_M$ values of Eq. (6). It should be noted here that an approximate M-shell initial vacancy distribution assumed to calculate $\bar{\omega}_M$, i.e., [0, 0, 0, 0.4, 0.6], was also used to obtain weighted averages of M-shell quantities discussed above, i.e., θ_M, ξ_M, and σ_{0M}.

IV. RESULTS AND DISCUSSION

The M-shell x-ray production cross sections were measured for 0.6–4.0-MeV proton impact on $_{72}$Hf, $_{73}$Ta, $_{74}$W, $_{75}$Re, $_{76}$Os, $_{77}$Ir, $_{78}$Pt, $_{79}$Au, $_{83}$Bi, and $_{90}$Th targets with energy steps of 0.1 and 0.2 MeV, below and above 1 MeV energy, respectively. The experimental M-shell x-ray production cross sections obtained in the present work,

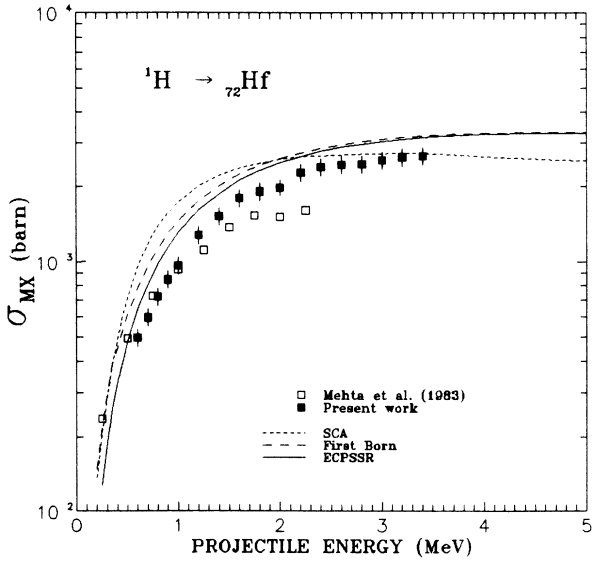

FIG. 5. M-shell x-ray production cross section for the hafnium target vs proton energy. The predictions of the ECPSSR theory (Refs. 3 and 40) (——), the first Born approximation (Refs. 38 and 42) (— — —), and the semiclassical SCA (- - -) of Hansteen *et al.* (Ref. 43) are shown. The present data are compared with the results of Mehta *et al.* (Ref. 22).

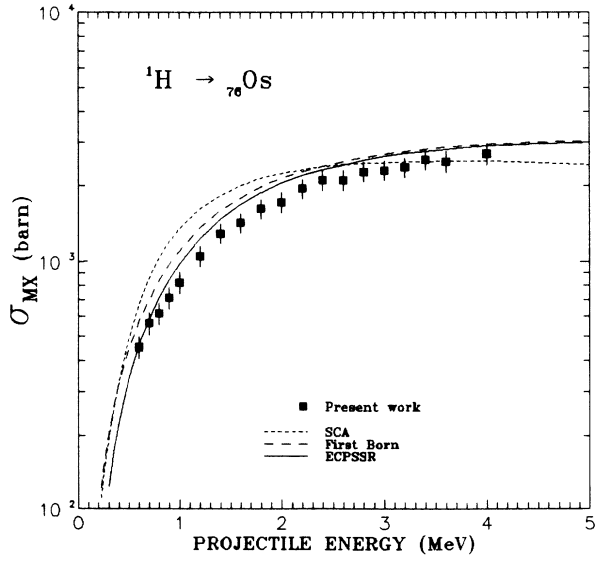

FIG. 6. M-shell x-ray production cross section for the osmium target vs proton energy. The curves are as in Fig. 5; no other data were found for this element in the studied 0.6–4-MeV energy range.

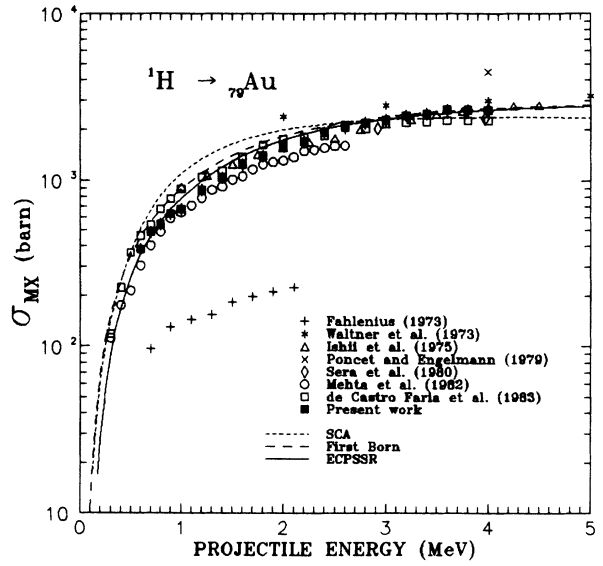

FIG. 7. M-shell x-ray production cross section for the gold target vs proton energy. The curves are as in Fig. 5; the other data are from Refs. 10, 11, 14, 17, 18, 20, and 21,

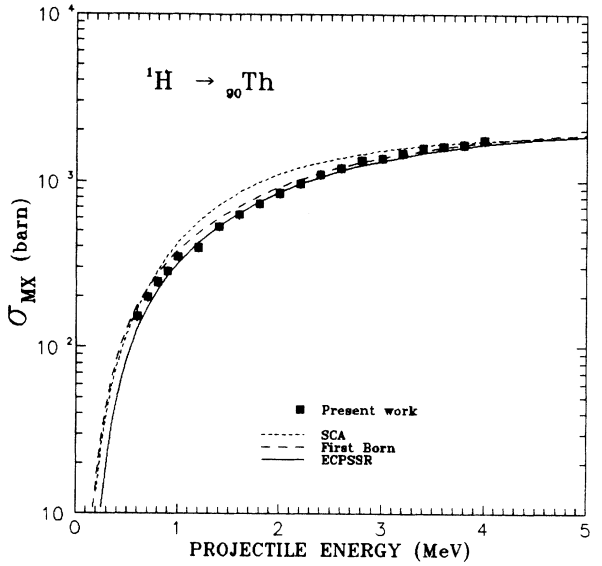

FIG. 9. M-shell x-ray production cross section for the thorium target vs proton energy. The curves are as in Fig. 5; no other data were found for this element in the studied 0.6–4-MeV energy range.

including estimated total uncertainties, are given in Table I.

In Figs. 5–9, the measured M-shell x-ray production cross sections, with theoretical predictions of the ECPSSR theory,[3,40] the first Born approximations[38,42] (PWBA plus the Oppenheimer-Brinkman-Kramers-Nikolaev theory) and the SCA of Hansteen *et al.*,[43] are shown for half of the studied elements (selected to represent the target elements from the interval of interest: $72 \leq Z_2 \leq 90$), namely, $_{72}$Hf, $_{76}$Os, $_{79}$Au, $_{83}$Bi, and $_{90}$Th.

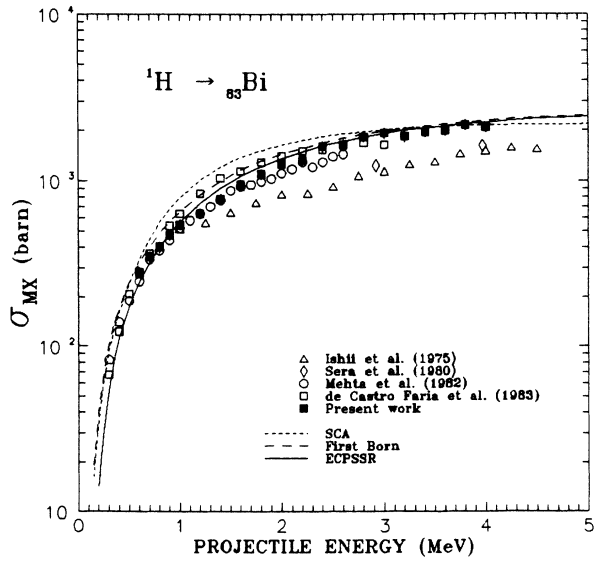

FIG. 8. M-shell x-ray production cross section for the bismuth target vs proton energy. The curves are as in Fig. 5; the other data are from Refs. 14, 18, 20, and 21,

We found in the literature cross sections for M-x-ray production by protons in hafnium,[8,19,22] tantalum,[15,19] tungsten,[9,19] platinum,[6,16,19] gold,[6,10,11,14,17–21,25] bismuth,[6,14,15,20,21,25] thorium,[25] and none in the $Z_2 = 75–77$ elements. Only the data of Refs. 10, 11, 14–18, and 20–22, which overlap our range of proton energies, are compared with our measurements as follows. In $_{72}$Hf of Fig. 5, the cross section of Mehta *et al.*[22] are, within experimental uncertainties in agreement with ours except for $E_1 > 1$ MeV where they fall about 20% below. In $_{73}$Ta, the data of Nikolaev *et al.*[15] exceed ours by 50% at 1 MeV and as much as a factor of 2 at 0.6 MeV. The cross sections of Petukhov *et al.*[16] in $_{78}$Pt are also larger than ours but only by 10–15 %. In $_{79}$Au of Fig. 7, Ishii *et al.*[14] reported cross sections within experimental uncertainties with ours except of about 1 MeV energy where they are some 20% higher. The gold data of Mehta *et al.*[20] agree with ours within experimental uncertainties at 1 MeV but fall up to 20% both at 0.6 MeV and above 2 MeV energy. The gold results of de Castro Faria *et al.*[21] are within experimental uncertainties with our data in the range of 2–3 MeV, but they are systematically higher towards lower energies (up to 20%) and some 15% lower for $E_1 > 3$ MeV, where they coincide with data of Sera *et al.*[18] From the overall comparison of gold data, the cross sections of Waltner *et al.*,[11] which exceed ours by factors 1.5–1.15 in the 2–4-MeV range, of Poncet and Engelmann,[17] which is 70% larger then ours at 4 MeV, and, especially, of Fahlenius,[10] which are below

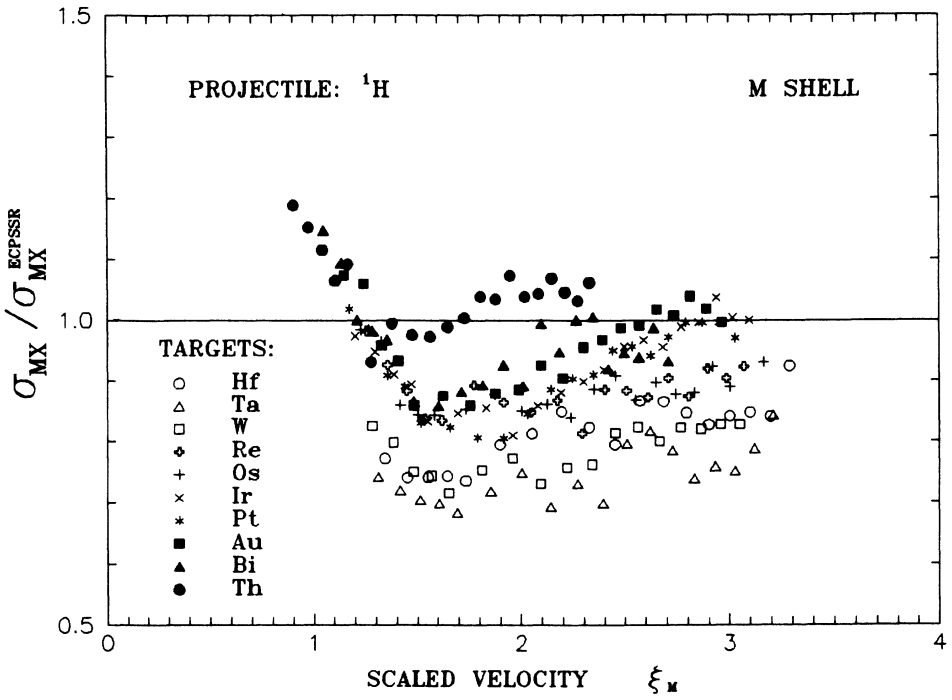

FIG. 10. $\sigma_{MX}/\sigma_{MX}^{ECPSSR}$ ratios for all elements studied in this work as a function of the average M-shell scaled velocity ξ_M. The symbols used to mark different elements are identified in the figure.

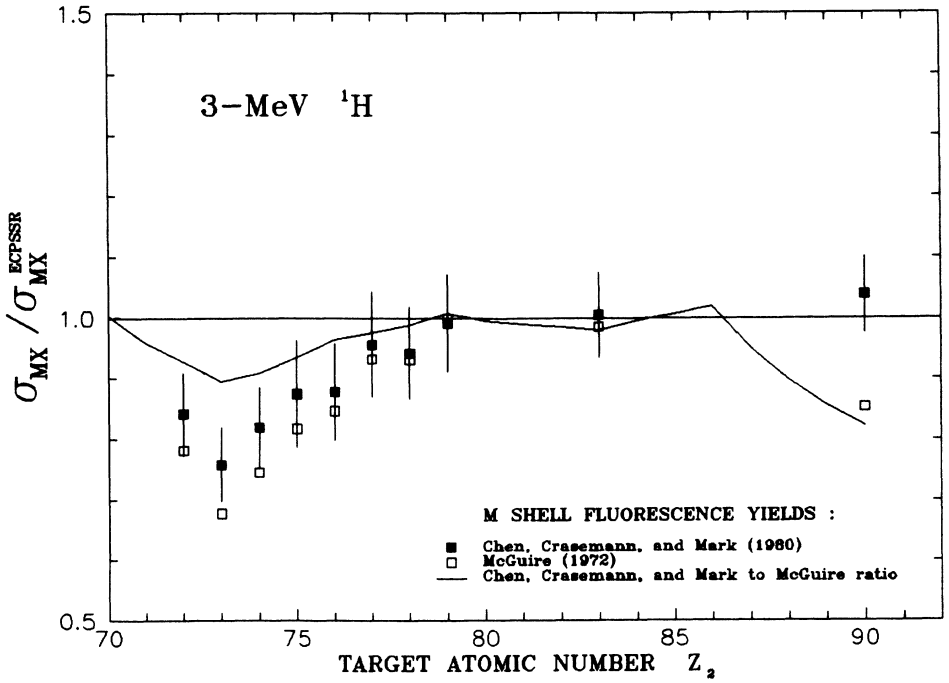

FIG. 11. $\sigma_{MX}/\sigma_{MX}^{ECPSSR}$ ratios for all studied elements and 3-MeV protons for two sets of the M-shell Coster-Kronig and fluorescence yields, namely, of Chen *et al.* (Ref. 46) (■) and McGuire (Ref. 47) (□). The ratios of the average M-shell fluorescence yields $\bar{\omega}_M$ of Eq. (6) calculated according to Chen *et al.* and McGuire are joined using the solid line to exhibit trends of these ratios with Z_2.

ours by factors 5–7 in the 0.7–2.1-MeV range, most probably had large systematic errors. In $_{83}$Bi of Fig. 8, both data of Refs. 20 and 21 are in essential agreement (on average ±15%) with ours, but for $E_1 > 2$ MeV the data of Mehta *et al.*[20] fall some 20% below, while the results of de Castro Faria *et al.*[21] are 20% higher in the 1–2-MeV range. The bismuth cross sections of Ishii *et al.*[14] fall systematically 30–40 % below even though the cross sections of Sera *et al.*[18] are only 15–20 % smaller. In the overall comparison of all our data with those available from the literature, barring apparently erroneous measurements of Refs. 10, 11, and 17 for gold and, most probably erroneous data of Ref. 15 for tungsten, our cross sections typically *agree* with mean of others at the lowest energy of 0.6 MeV and are some 20–30 % *above* in the 2–4-MeV range.

The measured M-shell x-ray production cross sections are compared, systematically and in a magnified manner, with predictions of the ECPSSR theory in Fig. 10, where $\sigma_{MX}/\sigma_{MX}^{\mathrm{ECPSSR}}$ ratios were plotted for all studied elements versus average M-shell scaled velocity ξ_M. Generally, very good agreement is observed for heavier targets, an average ±15%, however, the experimental cross sections for the lightest targets, namely, $_{72}$Hf, $_{73}$Ta, and $_{74}$W are systematically 20–30 % smaller than the ECPSSR predictions. Given that the ECPSSR theory reproduces the energy dependence of measured cross sections very well, especially for higher energies, the observed discrepancies for lighter targets may be attributed to the adopted M-shell fluorescence yields and Coster-Kronig factors. To clarify this point, in Fig. 11, the ratios $\sigma_{MX}/\sigma_{MX}^{\mathrm{ECPSSR}}$ for 3-MeV proton impact are plotted versus target atomic number and, additionally since σ_{MX} cross sections scale as $\bar{\omega}_M$ values, the ratios of the average M-shell fluorescence yields calculated using Eq. (6) according to Chen *et al.*[46] and McGuire[47] are shown. As can be seen in this figure, the relativistic M-subshell Coster-Kronig and fluorescence yields of Chen *et al.* yield better agreement of the ECPSSR theory with present experiment than values of McGuire would give. Furthermore, the atomic number dependence of $\bar{\omega}_M$ ratios is quite the same as for $\sigma_{MX}/\sigma_{MX}^{\mathrm{ECPSSR}}$, which suggests that the observed discrepancies between the ECPSSR ionization theory and x-ray production measurements for the lightest targets may originate from some deficiencies in calculation of M-subshell transition rates. It is interesting to note that the mentioned discrepancies observed for $_{72}$Hf, $_{73}$Ta, and $_{74}$W coincide with the atomic number region where the calculations of Chen *et al.* and McGuire differ essentially due to a very different estimation as to where the strong $M_4-M_5N_{6,7}$ Coster-Kronig transitions start to be energetically forbidden, namely, already[46] for $Z_2=74$ or as late[47] as $Z_2=78$. The near equality of $\bar{\omega}_M$ from Refs. 46 and 47 for the $Z_2=80-85$ targets is probably fortuitous because the slope discontinuities of McGuire's Auger widths with Z_2 for these elements; the decrease in the Chen *et al.*/McGuire ratio in Fig. 11 for $Z_2 > 85$ underscores the difference between the relativistic[46] and nonrelativistic[47] calculations.

Finally, in Fig. 12, the universal M-shell ionization

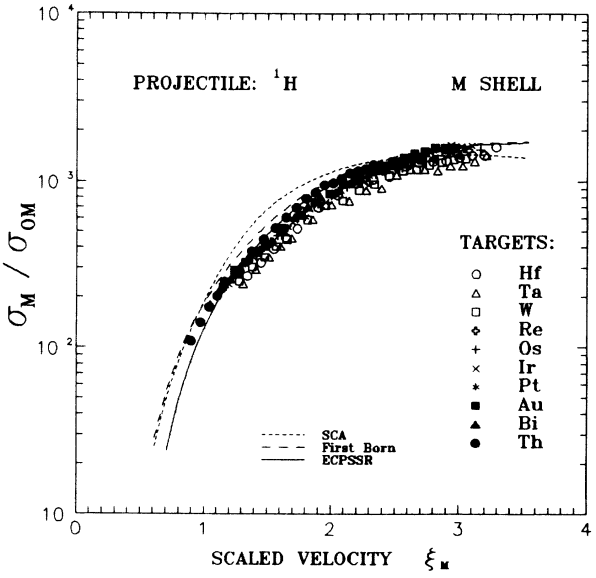

FIG. 12 Universal M-shell ionization cross sections σ_M/σ_{0M} (see Sec. III) for protons on all elements studied in this work (the symbols used are labeled in the figure), plotted vs average M-shell scaled velocity ξ_M. The predictions of the universal M-shell ionization cross section (for $\theta_M=0.45$) according to the ECPSSR theory (Refs. 3 and 40) (——), the first Born approximation (Refs. 38 and 42) (— — —), and the semiclassical approximation (- - -) of Hansteen *et al.* (Ref. 43) are shown.

cross sections σ_M/σ_{0M} are plotted versus average M-shell scaled velocity ξ_M, where σ_M cross sections were obtained from measured x-ray production data using $\bar{\omega}_M$ of Eq. (6) with fluorescence yields of Chen *et al.*[46] The ECPSSR theory gives the best prediction of M-shell ionization cross sections versus ξ_M, despite a slight systematical overestimation (about 15%) of the present experimental data by the ECPSSR theory for $\xi_M \geq 1.2$ (see also Fig. 10). However, further new data are needed to test this theory, especially because our data for $\xi_M \geq 1.2$ are 20–30 %, on the average, larger than existing data of others and since at lowest ξ_M of Figs. 10 and 11 the available cross sections are typically an additional 20% larger than the ECPSSR calculations.

V. CONCLUSIONS

The M-shell x-ray production cross sections for ten heavy elements ($_{72}$Hf–$_{90}$Th) were measured, with the total experimental uncertainities of 7–10 %, using protons of energy 0.6–4.0 MeV. Generally, a very good agreement (±15%) of the present experimental results with the predictions of the ECPSSR theory was observed. Some systematical discrepancies (up to 30%) were found for the lightest elements ($_{72}$Hf, $_{73}$Ta, and $_{74}$W), buth they could be attributed to the M-shell Coster-Kronig and fluorescence yields used to convert the theoretical M-subshell

ionization cross section to the total M-x-ray production cross section. It has been demonstrated that the relativistic M-subshell Coster-Kronig and fluorescence yields of Chen *et al.*[46] seem to be more reliable than those of McGuire,[47] but, probably, some deficiency still exists near $Z_2=74$, where the strong $M_4-M_5N_{6,7}$ Coster-Kronig transitions become energetically forbidden.

ACKNOWLEDGMENTS

The authors are indebted to the EG-5 Van de Graaff accelerator staff for their kind collaboration during the measurements. One of the authors (M. P.) wishes to acknowledge the support provided by the CPBP 01.09 Program.

[1]E. Merzbacher and H. Lewis, *Handbuch der Physik,* edited by S. Flügge (Springer-Verlag, Berlin, 1958), Vol. 34, p. 146.

[2]J. Bang and J. M. Hansteen, K. Dansk. Vidensk. Selsk. Mat. -Fys. Medd. **31**, (13) (1959); L. Kocbach, J. Phys. B **9**, 2269 (1976); D. Trautmann, F. Rösel, and G. Baur, Nucl. Instrum. Methods **214**, 21 (1983).

[3]W. Brandt and G. Lapicki, Phys. Rev. A **23**, 1717 (1981); G. Lapicki, Bull. Am. Phys. Soc. **26**, 1310 (1981).

[4]C. H. Rutledge and R. L. Watson, At. Data Nucl. Data Tables **12**, 195 (1973); R. K. Gardner and T. J. Gray, *ibid.* **21**, 515 (1978); **24**, 281 (E) (1979); H. Paul and J. Muhr, Phys. Rep. **135**, 47 (1986); G. Lapicki, J. Phys. Chem. Ref. Data **18**, 111 (1989).

[5]T. L. Hardt and R. L. Watson, At. Data Nucl. Data Tables **17**, 107 (1976); R. S. Sokhi and D. Crumpton, *ibid.* **30**, 49 (1984).

[6]R. C. Jopson, H. Mark, and D. C. Swift, Phys. Rev. **127**, 1612 (1962).

[7]J. M. Khan, D. L. Potter, and R. D. Worley, Phys. Rev. **135**, A511 (1964); **139**, A1735 (1965).

[8]P. B. Needham, Jr. and B. D. Sartwell, Phys. Rev. A **2**, 27 (1970); **2**, 1686 (1971).

[9]K. Shima, I. Makino, and M. Sakisaka, J. Phys. Soc. Jpn. **30**, 611 (1971).

[10]A. Fahlenius, *Electrical and Nuclear Technology* (Technical Research Centre of Finland, Helsinki, 1973), Vol. 3, p. 1.

[11]A. W. Waltner, D. M. Peterson, G. A. Bissinger, A. B. Baskin, C. E. Busch, P. Nettles, W. R. Scates, and S. M. Shafroth, *International Conference on Inner-Shell Ionization Phenomena, Atlanta, 1972,* edited by R. Fink, S. T. Manson, M. Palms, and P. V. Rao (U.S. AEC, Oak Ridge, TN, 1973), p. 1080.

[12]C. E. Busch, A. B. Baskin, P. H. Nettles, S. M. Shafroth, and A. W. Waltner, Phys. Rev. A **7**, 1601 (1973).

[13]S. T. Thornton, R. C. McKnight, and R. R. Karlowicz, Phys. Rev. A **10**, 219 (1974).

[14]K. Ishii, S. Morita, H. Tawara, H. Kaji, and T. Shiokawa, Phys. Rev. A **11**, 119 (1975).

[15]V. S. Nikolaev, V. P. Petukhov, E. A. Romanovsky, V. A. Sergeev, I. M. Kruglova, and V. V. Beloshitsky, in *Proceedings of the Ninth International Conference on the Physics of Electronic and Atomic Collisions, Seattle, 1975,* edited by J. R. Risley and R. Geballe (University of Washington, Seattle, 1975), p. 419.

[16]V. P. Petukhov, E. A. Romanovsky, I. M. Kruglova, V. S. Nikolaev, and V. A. Sergeev, in *Proceedings of the Tenth International Conference on the Physics of Electronic and Atomic Collisions, Paris, 1977,* edited by G. Watel (North-Holland, Amsterdam, 1978), p. 64.

[17]M. Poncet and C. Engelmann, Nucl. Instrum. Methods **159**, 455 (1979).

[18]K. Sera, K. Ishii, A. Yamedera, A. Kuwako, M. Kamiya, M. Sebata, S. Morita, and T. C. Chu, Phys. Rev. A **22**, 2536 (1980).

[19]M. Sarkar, H. Mommsen, W. Sarter, and P. Schurkes, J. Phys. B **14**, 3163 (1981).

[20]R. Mehta, J. L. Duggan, J. L. Price, F. D. McDaniel, and G. Lapicki, Phys. Rev. A **26**, 1883 (1982).

[21]N. V. de Castro Faria, F. L. Freire, Jr., A. G. de Pinho, and E. F. da Silveira, Phys. Rev. A **28**, 2770 (1983).

[22]R. Mehta, J. L. Duggan, J. L. Price, P. M. Kocur, F. D. McDaniel, and G. Lapicki, Phys. Rev. A **28**, 3217 (1983).

[23]R. Gowda and D. Powers, Phys. Rev. A **31**, 134 (1985).

[24]J. L. Price, J. L. Duggan, F. D. McDaniel, G. Lapicki, and R. Mehta, Phys. Rev. A **37**, 365 (1988).

[25]J. D. Gressett, D. K. Marble, F. D. McDaniel, J. L. Duggan, J. F. Culwell, and G. Lapicki, Nucl. Instrum. Methods B **40/41**, 116 (1989).

[26]M. Pajek, A. P. Kobzev, R. Sandrik, R. A. Ilkhamov, and S. H. Khusmurodov, Nucl. Instrum. Methods B **42**, 346 (1989).

[27]V. B. Zlokazov, Comput. Phys. Commun. **28**, 27 (1982).

[28]H. H. Andersen and J. F. Ziegler, *The Stopping and Ranges of Ions in Matter* (Pergamon, New York, 1977), Vol. 3.

[29]W. M. J. Veigele, At. Data Tables **5**, 51 (1973).

[30]J. L'Ecuyer, J. A Davies, and N. Matsunami, Nucl. Instrum. Methods **160**, 337 (1979).

[31]E. Huttel, W. Arnold, H. Baumgart, and G. Clausnitzer, Nucl. Instrum. Methods B **12**, 193 (1985).

[32]Y. Inagaki, K. Shima, and H. Meazawa, Nucl. Instrum. Methods B **27**, 353 (1987).

[33]M. H. Chen, B. Crasemann, and H. Mark, Phys. Rev. A **27**, 2358 (1983).

[34]P. M. Kocur, J. L. Duggan, R. Mehta, J. Robbins, and R. D. McDaniel, IEEE Trans. Nucl. Sci. **NS-30**, 1580 (1983).

[35]V. V. Sizov and N. M. Kabachnik, J. Phys. B **13**, 1601 (1980); B. Cleff, Acta Phys. Polonica A **61**, 285 (1982).

[36]J. Wigger, H. Altevogt, M. Brüssermann, G. Richter, and B. Cleff, J. Phys. B **17**, 4721 (1984).

[37]W. Mehlhorn, in *Proceedings of the International Seminar on High-Energy Ion-Atom Collision Processes, Debrecen, Hungary, 1981,* edited by D. Berényi and G. Hock (Elsevier, Amsterdam, 1982), p. 83.

[38]D. E. Johnson, G. Basbas, and F. D. McDaniel, At. Data Nucl. Data Tables **24**, 1 (1979).

[39]D. E. Johnson, F. D. McDaniel, and G. Basbas, IEEE Trans. Nucl. Sci. **NS-26**, 1177 (1979).

[40]G. Lapicki and F. D. McDaniel, Phys. Rev. A **22**, 1896 (1980); **23**, 975 (E) (1981).

[41]F. D. McDaniel, Nucl. Instrum. Methods. **214**, 57 (1983).

[42]V. S. Nikolaev, Zh. Eksp. Teor. Fiz. **51**, 1263 (1966) [Sov. Phys.—JETP **24**, 847 (1967)].

[43]J. M. Hansteen, O. M. Johnsen, and L. Kocbach, At. Data

Nucl. Data Tables **15**, 305 (1975).
[44]W. Bambynek, B. Crasemann, R. W. Fink, H.-U. Freund, H. Mark, C. D. Swift, R. E. Price, and P. V. Rao, Rev. Mod. Phys. **44**, 716 (1972).
[45]M. O. Krause, Phys. Rev. A **22**, 1958 (1980).
[46]M. H. Chen, B. Crasemann, and H. Mark, Phys. Rev. A **21**, 449 (1980); **27**, 2989 (1983).
[47]E. J. McGuire, Phys. Rev. A **5**, 1043 (1972).